

Complete set of elastic constants of α -quartz at high pressure: A first-principles study

Hajime Kimizuka,^{1,2,*} Shigenobu Ogata,^{1,3} Ju Li,⁴ and Yoji Shibutani^{1,3}

¹Department of Mechanical Engineering, Osaka University, Osaka 565-0871, Japan

²Engineering Technology Division, The Japan Research Institute, Limited, Tokyo 102-0082, Japan

³Center for Atomic and Molecular Technologies, Osaka University, Osaka 565-0871, Japan

⁴Department of Materials Science and Engineering, Ohio State University, Columbus, Ohio 43210, USA

(Received 14 June 2006; published 20 February 2007)

We calculated all the independent elastic constants of α -quartz under hydrostatic pressure up to 20 GPa using density functional theory. The predicted pressure-dependent elastic behavior differs significantly from a recent Brillouin spectroscopy measurement [E. Gregoryanz *et al.*, Phys. Rev. Lett. **84**, 3117 (2000)], but is consistent with x-ray data in the literature.

DOI: [10.1103/PhysRevB.75.054109](https://doi.org/10.1103/PhysRevB.75.054109)

PACS number(s): 61.66.-f, 62.20.Dc, 71.15.Mb

I. INTRODUCTION

Quartz, one of the common allotropes of SiO₂ and the most abundant mineral in Earth's crust, is an important material in diverse fields. Quartz-crystal oscillators are used in many devices such as electronic watches, computers, and cellular phones, as a reference signal generator. Also, the quartz-crystal microbalance (QCM) technique¹ is widely used in biochemical and biomedical applications to sense molecular adsorption at solid-gas or solid-liquid interfaces. These applications are based on the inverse piezoelectric effect of quartz and its characteristic elastic behavior associated with mechanical compression or tension.

The effect of pressure on the propagation of elastic waves in materials is essential for predicting and understanding interatomic forces, mechanical stability,² phase transition mechanisms,³ dynamic fracture,⁴ earthquakes, and the internal structures of Earth. However, not much is known about the elasticity of solids at high pressure, since measurement of the elastic constants is challenging under high pressure. Traditional methods have been applied only to moderate pressures. (Ultrasonic measurements are generally limited to a few gigapascals and Brillouin spectroscopy has been applied up to 25 GPa.) While numerous experimental studies of the elastic constants of quartz have been performed,^{5,6} few entailed the hydrostatic pressure P as a variable.⁷ Gregoryanz *et al.*⁸⁻¹⁰ recently reported the Brillouin spectroscopy measurements of the single-crystal elastic moduli of α -quartz to above $P=20$ GPa using diamond-anvil cell, which yielded the values of the individual elastic constants as functions of pressure.

On the other hand, a number of calculations have been performed on the mechanical properties of various high-pressure and/or temperature silica phases, including α -quartz, via molecular-dynamics and first-principles calculation approaches (see, for example, Refs. 11–18). Modern *ab initio* modeling is expected to provide a good description of the elastic behavior of condensed phases¹⁹ over a wide pressure range. However, to our knowledge, a systematic explanation has not been available on the pressure evolution of the complete set of elastic constants of quartz, since such calculations of the individual elastic constants are quite elaborate for systems with relatively low symmetries.

In the present study, we report the individual high-pressure elastic constants of quartz as determined from first-principles variable-cell-shape calculations. The main objective of the present article is to provide results of the density-functional-theory (DFT) calculations that can be used to evaluate quantitatively the high-pressure elasticity of quartz up to 20 GPa, and to investigate the microscopic mechanism for the elastic-constant behavior associated with compression. The data thus obtained can be compared with the numerous experimental compressibility data and also the elastic constants reported by Gregoryanz *et al.*⁸

II. SIMULATION TECHNIQUES

We use the Vienna *ab initio* simulation package (VASP),²⁰ with addition of a variable-cell-shape algorithm under applied stress. Gibbs free-energy minimization under an applied pressure at $T=0$ K is performed using the projector-augmented-wave (PAW) method.^{21,22} For the exchange-correlation potential, the local-density approximation (LDA) functional given by Ceperley and Alder²³ and parametrized by Perdew and Zunger²⁴ is used. The calculations employ the primitive cell of α -quartz (space group $P3_121$),²⁵ containing nine atoms. A plane-wave basis set with 1400 eV kinetic-energy cutoff is adopted. Such a large energy cutoff is found to be necessary to achieve convergence for all the elastic-constant components. We also employ a $4 \times 4 \times 4$ Γ -centered \mathbf{k} mesh (13 irreducible \mathbf{k} points) for carrying out the Brillouin-zone integration using the tetrahedron method with Blöchl correction.²⁶ We increase the pressure in 0.5 GPa increments for pressures up to 20 GPa. Forces on atoms and internal pressure are calculated, and atom positions and cell parameters are allowed to relax using a conjugate gradient technique until their residual forces have converged to less than 0.0005 eV/Å.

The definition of elastic constants $C_{ijkl}(X)$ at a finite-stress state X is given by the free-energy expansion,²⁷

$$F(Y) \equiv F(X) + \Omega(X) \left[\tau_{ij}(X)(\eta_X^Y)_{ij} + \frac{1}{2} C_{ijkl}(X)(\eta_X^Y)_{ij}(\eta_X^Y)_{kl} \right] + O[(\eta_X^Y)^3], \quad (1)$$

where η_X^Y is the Lagrangian strain connecting states X and Y ,

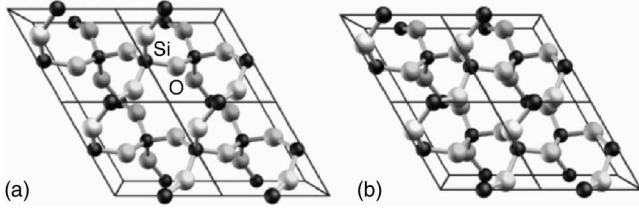


FIG. 1. Effect of pressure on the structure of α -quartz as viewed down the c axis at (a) 0 GPa and (b) 20 GPa. The oxygen and silicon atoms are represented by the gray and black spheres, respectively.

$\Omega(X)$ is the volume of X , and $F(X)$, $F(Y)$ are the Helmholtz free energies of X and Y . This definition is convenient because it can be shown that $\tau_{ij}(X)$ is precisely the physical “force per unit area” at X if at equilibrium, and both $\tau_{ij}(X)$ and $C_{ijkl}(X)$ can be evaluated at X without requiring an extra reference state.

In our calculations, a complete set of C_{ij} ’s (in Voigt notation) are computed from numerical derivatives of the internal energy with respect to strain. The symmetry of the crystal structures of α -quartz is trigonal, which means that there are six independent elastic constants. The total energy is calculated in the strained lattice for several values of the magnitude of the linear strain ϵ . Generally, six values of ϵ are chosen, $\epsilon=0.0025, 0.004, 0.005, 0.006, 0.0075, \text{ and } 0.01$. The unit cell is slightly deformed with every ϵ in different directions, each corresponding to a certain component of elastic constants, and then the atomic coordinates are allowed to relax. C_{ij} ’s are then obtained by fitting a polynomial to the total energy F as a function of $\eta(\epsilon)$, and then taking the quadratic derivatives $\partial^2 F / \partial \eta^2$.

In strained crystals, the sound velocities correspond to the effective elastic constants or Birch coefficients (B_{ij}) rather than C_{ij} (see, for example, Refs. 28 and 29). The equality $B_{ij}=C_{ij}$ holds only at zero external stress. In order to compare with the experimental data, the B_{ij} ’s are calculated from the following equation:³⁰

$$B_{ijkl} = C_{ijkl} + P(\delta_{ij}\delta_{kl} - \delta_{ik}\delta_{jl} - \delta_{il}\delta_{jk}), \quad (2)$$

where P denotes the internal hydrostatic pressure and δ_{ij} the Kronecker delta.

III. RESULTS AND DISCUSSION

A. Structural variations with pressure

The lattice parameters (a and c) and unit-cell volume (Ω) of α -quartz at ambient pressure are evaluated using the DFT calculations. The obtained values are $a_0=4.863$ (4.9134) Å, $c_0=5.364$ (5.4052) Å, and $\Omega_0=109.9$ (113.01) Å³, where the numbers in parentheses are the experimental values²⁵ at 298 K. For the present method, the calculated theoretical values are found to be slightly small (within 1% for lattice parameters and 3% for unit-cell volume), but fairly close to those obtained from the neutron-diffraction data.²⁵ With increasing pressure from 0 to 20 GPa, the unit-cell parameters decrease continuously with pressure and the system succes-

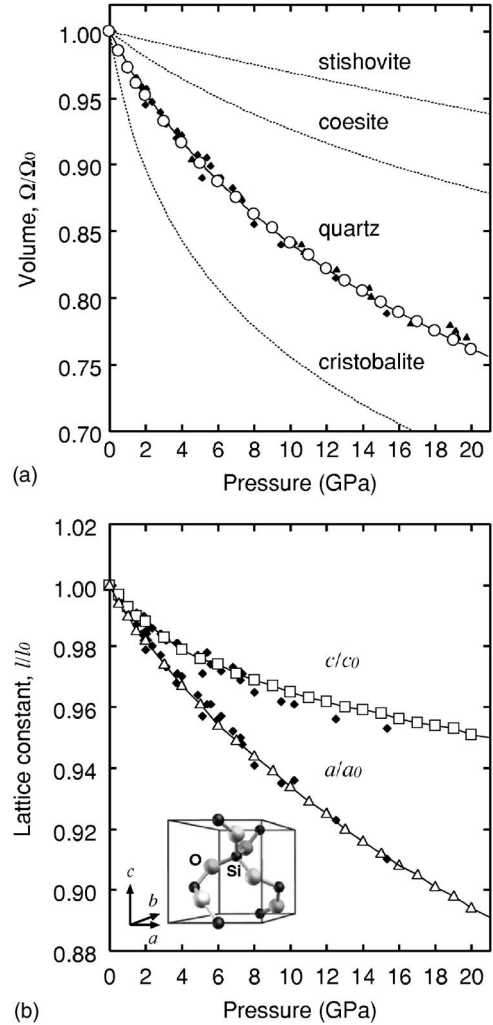


FIG. 2. Pressure evolution of the (a) unit-cell volume and (b) lattice constants of α -quartz. (a) The open circles represent data from the DFT calculations, and the solid curve is the best-fit Birch-Murnaghan equation of state with parameters $K_0=37.7(3)$ GPa and $K'_0=4.9(1)$, where K_0 and K'_0 denote the zero pressure bulk modulus and its pressure derivative, respectively. The x-ray-diffraction data (solid symbols) are from Refs. 31–36. For comparison, the pressure-volume curves for cristobalite ($K_0=11.5$, $K'_0=9.0$ in Ref. 37), coesite ($K_0=96$, $K'_0=8.4$ in Ref. 38), and stishovite ($K_0=313$, $K'_0=2.8$ in Ref. 39) are shown as dotted lines. (b) The open triangles and squares represent normalized lattice lengths a/a_0 and c/c_0 obtained from the DFT calculations, respectively. The x-ray-diffraction data (solid symbols) are from Refs. 31–35.

sively undergoes compressive deformation. Also, the trigonal phase of quartz survives compression up to the applied pressure of 20 GPa under the present symmetry conditions, as shown in Fig. 1.

From the first-principles total-energy minimization calculations, the theoretical pressure-volume data were obtained. Figure 2(a) shows the volume compressibility curve, along with the x-ray-diffraction data from Refs. 31–36. It is noteworthy that our theoretical data obtained from the DFT calculations are in good agreement with the experimental data under hydrostatic pressure. Figure 2(b) shows the axial compressibility curves for a and c axes. The compressibility of

TABLE I. Calculated values for elastic constants (C_{ij} in GPa) and Birch coefficients (B_{ij} in GPa), bulk modulus (K in GPa), and the anisotropy of linear compressibility (β_2 in 10^{-3} GPa $^{-1}$) of α -quartz, together with experimental values. At 0 GPa, the equality $B_{ij}=C_{ij}$ holds.

	$P=0$ GPa			5 GPa	10 GPa	15 GPa	20 GPa
	Expt. ^a	Expt. ^b	Calc.				
C_{11}	86.8	87.7	81.1	96.6	132.6	164.4	176.4
C_{33}	106.4	106.3	104.8	163.1	233.4	269.8	294.9
C_{44}	58.0	59.0	49.7	62.7	67.0	80.8	69.6
C_{66}	39.8	40.5	36.4	31.5	38.3	61.0	57.5
C_{12}	7.2	6.8	8.3	33.6	56.0	42.4	61.4
C_{13}	12.0	12.3	7.5	21.3	49.6	54.3	69.5
C_{14}	17.9	18.7	23.3	3.7	-4.1	-6.8	-19.9
B_{11}				91.6	122.6	149.4	156.4
B_{33}				158.1	223.4	254.8	274.9
B_{44}				57.7	57.0	65.8	49.6
B_{66}				26.5	28.3	46.0	37.5
B_{12}				38.6	66.0	57.4	81.4
B_{13}				26.3	59.6	69.3	89.5
B_{14}				3.7	-4.1	-6.8	-19.9
K	37.5	37.8	34.4	56.3	88.2	98.1	114.9
β_2	2.51	2.47	2.48	2.82	2.70	2.72	2.57

^aReference 5.

^bReference 6.

quartz is anisotropic and a axis is more compliant than c axis. Also, our theoretical data are found to agree well with the experimental data both for a and c , as indicated in Fig.

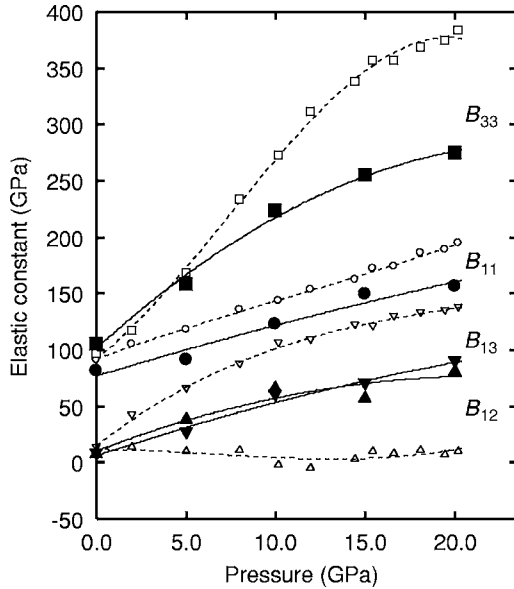


FIG. 3. Pressure evolution of the Birch coefficients of α -quartz: B_{11} (solid circle), B_{33} (solid square), B_{12} (solid triangle), and B_{13} (solid inverted triangle). The Brillouin scattering experimental data (small open symbols) are from Ref. 8, where the B_{12} values are not directly shown, and are thus derived from the equation $B_{12}=B_{11}-2B_{66}$.

2(b). This result suggests that our calculations have an ability to satisfactorily reproduce the anisotropic compression behavior of quartz in this pressure range.

B. Elastic constants

The elastic constants (C_{ij}) of quartz are evaluated under pressures from 0 to 20 GPa using the DFT calculations. The obtained C_{ij} values are given in Table I, and the Birch coefficients B_{ij} derived from Eq. (2) are also tabulated. We have included the experimental values^{5,6} at ambient pressure for comparison.

At 0 GPa, our calculated values are in good agreement with the experimental data. With increasing pressure up to 20 GPa, the B_{11} , B_{33} , B_{12} , and B_{13} values tend to increase, while B_{44} and B_{66} change gradually in this pressure range. Figure 3 displays the pressure evolution of B_{11} , B_{33} , B_{12} , and B_{13} , together with experimental values reported by Gregoryanz *et al.*⁸ (According to Ref. 10, the C_{ij} 's plotted in Ref. 8 are actually B_{ij} 's.) Similar monotonous pressure dependence is observed; however, their magnitudes are quite different. In particular, the discrepancy of B_{33} amounts to approximately 110 GPa at pressure of 20 GPa. Also, the B_{12} 's obtained from the experiment change little in this pressure range and exhibit a very low magnitude compared with the other components, whereas B_{12} and B_{13} increase similarly in our DFT data. In addition, a recent DFT calculation¹⁸ indicates a similar evolution with pressure and a large discrepancy between the experimental and the theoretical values of elastic constants.

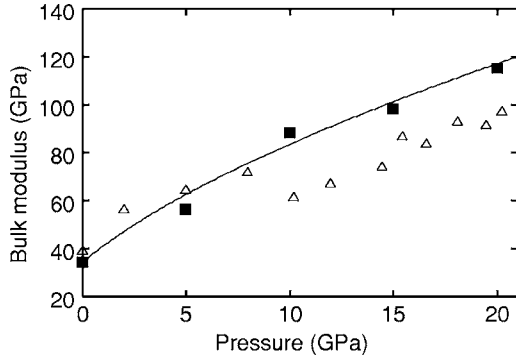


FIG. 4. Pressure evolution of the bulk modulus of α -quartz. The DFT values derived from Eq. (4) are indicated as solid squares. The solid curve represents the numerical derivative, $-dP/d \ln \Omega$. The Brillouin scattering experimental values (open triangles) are from Ref. 8.

In most materials, elastic constants change with temperature and the possibility that the above discrepancy comes from the difference in temperature conditions is considered; the DFT data are obtained at zero temperature, while the Brillouin scattering experiment¹⁰ is conducted at ambient temperature. However, according to the ultrasonic measurements⁷ of α -quartz at 77 and 298 K under ambient pressure, the individual elastic constants only slightly vary at low-temperature region below 298 K and the differences in each C_{ij} value are within 0.3–3.4 GPa. They are orders of magnitude significantly smaller than the pressure evolutions of elastic constants, and thus the effect of temperature can be almost ignored in the present case.

In a trigonal crystal, the connection between pressure increment and instantaneous strain is given by

$$-dP \begin{pmatrix} 1 \\ 1 \\ 1 \end{pmatrix} = \begin{pmatrix} B_{11} & B_{12} & B_{13} \\ B_{12} & B_{11} & B_{13} \\ B_{13} & B_{13} & B_{33} \end{pmatrix} \begin{pmatrix} da/a \\ da/a \\ dc/c \end{pmatrix}. \quad (3)$$

The bulk modulus (K) for trigonal crystals yields the combination of Birch coefficients,

$$K = \frac{B_{33}(B_{11} + B_{12}) - 2B_{13}^2}{2B_{33} + B_{11} + B_{12} - 4B_{13}}, \quad (4)$$

from Eq. (3) and $K \equiv -dP/d \ln \Omega$. According to Eq. (4), the K values derived from the B_{ij} 's at various pressures are also tabulated in Table I. On the other hand, we can determine K by another way from fitting a polynomial to the pressure dependence of $\ln \Omega$ based on Fig. 2(a). With the best-fit coefficients of a third-order polynomial, K ($=-dP/d \ln \Omega$) is calculated as a function of P . The obtained values are 34.2, 62.7, 83.6, 101.3, and 117.1 GPa at pressures of 0, 5, 10, 15, and 20 GPa, respectively. Figure 4 shows the pressure evolution of the bulk modulus obtained in the analysis, along with the Brillouin scattering experimental data from Ref. 8. The numerical derivative of the pressure with respect to volume ($-dP/d \ln \Omega$) is shown as a solid curve as a function of P , based on the volume compressibility data. It is noteworthy that the K values derived from our B_{ij} values are slightly off

the curve at 5 and 10 GPa but sufficiently consistent with the volume compressibility data, while the K values obtained for experimental B_{ij} 's are fluctuating and strongly underestimated at high pressures.

C. Linear compressibility

The pressure dependence of the c/a ratio is also related to a combination of Birch coefficients, and thus, we make use of the linear compressibility β , i.e., the relative change in length of a line under hydrostatic pressure,^{40,41} to check the validity of the obtained B_{ij} 's. The linear compressibility of a trigonal crystal is in general anisotropic and can be derived from an expression similar to Eq. (3). In particular, the axial compressibilities β_a and β_c are of the form

$$\beta_a = -\frac{d \ln(a)}{dP} = \frac{B_{33} - B_{13}}{B_{33}(B_{11} + B_{12}) - 2B_{13}^2}, \quad (5)$$

$$\beta_c = -\frac{d \ln(c)}{dP} = \frac{B_{11} + B_{12} - 2B_{13}}{B_{33}(B_{11} + B_{12}) - 2B_{13}^2}. \quad (6)$$

Thus, the logarithmic pressure derivative of the axis ratio c/a , for which we use here the notation $\beta_2 \equiv d \ln(c/a)/dP$, is related to the anisotropy of the linear compressibility by the following equation:

$$\beta_2 = \beta_a - \beta_c, \quad (7)$$

where the coefficient β_2 can be expressed in terms of the Birch coefficients,

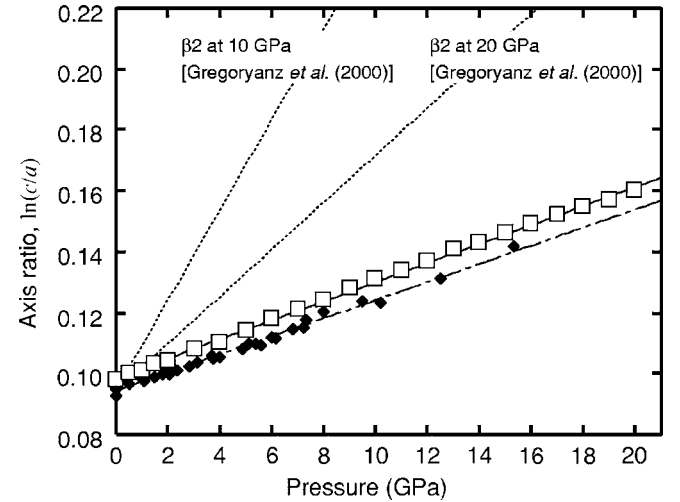


FIG. 5. Logarithmic axis ratio c/a for α -quartz as a function of pressure. The open squares represent the DFT data in this study, and the solid line is the best fit with the slope of $3.12 \times 10^{-3} \text{ GPa}^{-1}$. The x-ray-diffraction data (small solid symbols) are from Refs. 31–35, and the dot-dashed line is the best fit with the slope of $2.97 \times 10^{-3} \text{ GPa}^{-1}$. The dotted lines with the slope of 14.8 and 7.7 (in 10^{-3} GPa^{-1}) are based on the Birch coefficients of quartz measured in Ref. 8, at 10 and 20 GPa, respectively.

$$\beta_2 = \frac{B_{33} + B_{13} - B_{11} - B_{12}}{B_{33}(B_{11} + B_{12}) - 2B_{13}^2}. \quad (8)$$

We can determine β_2 by fitting a polynomial in finite strain to the pressure dependence of c/a . Thus, we have examined the consistency between β_2 derived from the c/a values and β_2 derived from the B_{ij} values.

Figure 5 displays the c/a ratio for quartz as a function of pressure, along with the diffraction data from Refs. 31–35. As clearly shown in Fig. 5, the logarithmic c/a ratio of quartz changes linearly with pressure both for the DFT and experimental data, and the slopes of their least-squares fits are almost the same ($3.12 \times 10^{-3} \text{ GPa}^{-1}$ for the DFT data and $2.97 \times 10^{-3} \text{ GPa}^{-1}$ for the experimental data).

Our predicted elastic constants for quartz as listed in Table I yield the β_2 values at various pressures. At ambient pressure, the β_2 values derived from the DFT data and the experimental data^{5,6} agree well with one another. At above 5 GPa, the β_2 values ranging from 2.57 to 2.82 (in 10^{-3} GPa^{-1}) apparently coincide with the above β_2 values over the pressure range up to 20 GPa. This suggests that the present B_{ij} 's are quantitatively consistent with the compressibility behavior, both for the experimental and DFT data. On the other hand, the B_{ij} values reported by Gregoryanz *et al.*⁸ yield the β_2 values ranging from 1.0 to 14.8 (in 10^{-3} GPa^{-1}) over the pressure range of 0 to 20 GPa, which are shown as dotted lines in Fig. 5. This large discrepancy in β_2 indicates that their B_{ij} values are not compatible with the compress-

ibility behavior in literature, and numerical reexamination may be needed.

IV. CONCLUSIONS

We have obtained the high-pressure elastic constants of α -quartz via state-of-the-art *ab initio* calculations with a variable-cell algorithm. A large discrepancy is found compared to the elastic constants/Birch coefficients obtained from Brillouin scattering measurements; however, our results are consistent with the experimentally established fact that the logarithmic axis ratio c/a of quartz changes linearly over a wide range of pressure. To this end, our calculations provide insight into the elastic behavior of quartz at high pressure, and it is noteworthy that first-principles techniques have such predictive capability.

ACKNOWLEDGMENTS

The authors express appreciation to H. Kaburaki for useful discussions on the computational methodology to evaluate the elastic constants under stress. S.O. acknowledges support by the Ministry of Education, Science, Sports and Culture, Grant-in-Aid for Scientific Research, 17760082, 2005. Work of J.L. is supported by Honda Research Institute USA, Inc., NSF DMR-0502711, AFOSR FA9550-05-1-0026, ONR N00014-05-1-0504, National Energy Technology Laboratory DE-AM26-04NT41817, and Ohio Supercomputer Center.

*Electronic address: kimizuka@comec.mech.eng.osaka-u.ac.jp

¹G. Sauerbrey, Z. Phys. **155**, 206 (1959).

²J. Li, K. J. Van Vliet, T. Zhu, S. Yip, and S. Suresh, Nature (London) **418**, 307 (2002).

³N. Binggeli and J. R. Chelikowsky, Phys. Rev. Lett. **69**, 2220 (1992); **71**, 2675 (1993).

⁴M. J. Buehler and H. J. Gao, Nature (London) **439**, 307 (2006).

⁵V. G. Zubov and M. M. Firsova, Kristallografiya **7**, 469 (1962) [Sov. Phys. Crystallogr. **7**, 374 (1962)].

⁶I. Ohno, J. Phys. Earth **43**, 157 (1995).

⁷H. J. McSkimin, P. Andreatch, Jr., and R. N. Thurston, J. Appl. Phys. **36**, 1624 (1965).

⁸E. Gregoryanz, R. J. Hemley, H. K. Mao, and P. Gillet, Phys. Rev. Lett. **84**, 3117 (2000).

⁹M. H. Müser and P. Schöffel, Phys. Rev. Lett. **90**, 079701 (2003).

¹⁰E. Gregoryanz, R. J. Hemley, H. K. Mao, R. E. Choen, and P. Gillet, Phys. Rev. Lett. **90**, 079702 (2003).

¹¹J. R. Chelikowsky, H. E. King, Jr., N. Troullier, J. Luis Martins, and J. Glinnemann, Phys. Rev. Lett. **65**, 3309 (1990).

¹²J. S. Tse and D. D. Klug, Phys. Rev. Lett. **67**, 3559 (1991).

¹³N. Binggeli, J. R. Chelikowsky, and R. M. Wentzcovitch, Phys. Rev. B **49**, 9336 (1994).

¹⁴H. Kimizuka, H. Kaburaki, and Y. Kogure, Phys. Rev. Lett. **84**, 5548 (2000).

¹⁵H. Kimizuka, H. Kaburaki, and Y. Kogure, Phys. Rev. B **67**, 024105 (2003).

¹⁶C. Campaña, M. H. Müser, J. S. Tse, D. Herzbach, and P.

Schöffel, Phys. Rev. B **70**, 224101 (2004).

¹⁷H. Kimizuka, S. Ogata, and Y. Shibusaki, Mater. Trans. **46**, 1161 (2005).

¹⁸N. Choudhury and S. L. Chaplot, Phys. Rev. B **73**, 094304 (2006).

¹⁹S. Ogata, J. Li, and S. Yip, Science **298**, 807 (2002).

²⁰G. Kresse and J. Furthmüller, Phys. Rev. B **54**, 11169 (1996).

²¹P. E. Blöchl, Phys. Rev. B **50**, 17953 (1994).

²²G. Kresse and D. Joubert, Phys. Rev. B **59**, 1758 (1999).

²³D. M. Ceperley and B. J. Alder, Phys. Rev. Lett. **45**, 566 (1980).

²⁴J. P. Perdew and A. Zunger, Phys. Rev. B **23**, 5048 (1981).

²⁵A. F. Wright and M. S. Lehmann, J. Solid State Chem. **36**, 371 (1981).

²⁶P. E. Blöchl, O. Jepsen, and O. K. Andersen, Phys. Rev. B **49**, 16223 (1994).

²⁷J. Wang, J. Li, S. Yip, S. Phillpot, and D. Wolf, Phys. Rev. B **52**, 12627 (1995).

²⁸D. C. Wallace, Rev. Mod. Phys. **37**, 57 (1965).

²⁹T. H. K. Barron and M. L. Klein, Proc. Phys. Soc. London **85**, 52 (1965).

³⁰J. Li, Ph.D. thesis, MIT, 2000.

³¹J. D. Jorgensen, J. Appl. Phys. **49**, 5473 (1978).

³²H. d'Amour, W. Denner, and H. Schulz, Acta Crystallogr., Sect. B: Struct. Crystallogr. Cryst. Chem. **B35**, 550 (1979).

³³L. Levien, C. T. Prewitt, and D. J. Weidner, Am. Mineral. **65**, 920 (1980).

³⁴R. M. Hazen, L. W. Finger, R. J. Hemley, and H. K. Mao, Solid

- State Commun. **72**, 507 (1989).
- ³⁵J. Glinnemann, Jr., H. E. King, Jr., H. Schulz, T. Hahn, S. J. L. Placa, and F. Dacol, *Z. Kristallogr.* **198**, 177 (1992).
- ³⁶K. J. Kingma, Ph.D. thesis, Johns Hopkins University, 1994; R. J. Hemley, C. T. Prewitt, and K. J. Kingma, *Rev. Mineral.* **29**, 41 (1994).
- ³⁷R. T. Downs and D. C. Palmer, *Am. Mineral.* **79**, 9 (1994).
- ³⁸L. Levien and C. T. Prewitt, *Am. Mineral.* **66**, 324 (1981).
- ³⁹N. L. Ross, J-F. Shu, R. M. Hazen, and T. Gasparik, *Am. Mineral.* **75**, 739 (1990).
- ⁴⁰J. F. Nye, *Physical Properties of Crystals: Their Representation by Tensors and Matrices* (Clarendon, Oxford, 1985).
- ⁴¹J. P. Franck and R. Wanner, *Phys. Rev. Lett.* **25**, 345 (1970).